Time-delay analysis of LISA gravitational wave data: Elimination of spacecraft motion effects

F. B. Estabrook,* Massimo Tinto,† and J. W. Armstrong‡
Jet Propulsion Laboratory, California Institute of Technology, Pasadena, California 91109
(Received 6 March 2000; published 25 July 2000)

LISA (Laser Interferometer Space Antenna) is a proposed mission which will use coherent laser beams exchanged between three remote spacecraft to detect and study low-frequency cosmic gravitational radiation. Modeling each spacecraft as moving almost inertially, rigidly carrying a laser, beam splitters and photodetectors, we previously showed how the measured time series of Doppler shifts of the six one-way laser beams between spacecraft pairs could be combined, with suitable time delays, to cancel exactly the otherwise overwhelming phase noise of the lasers. Three of the combinations synthesized data that could in principle be obtained if the spacecraft separations were very precisely equal, as in Michelson interferometry; seven other combinations offered possible design advantages and useful redundancy. Here we extend those results by presenting time-delay equations for Doppler data from the actual drag-free configuration envisaged for the LISA mission. Each spacecraft will carry two proof-masses, shielded within two non-inertial optical benches carrying lasers and photodetectors. In this full drag-free configuration there are now twelve Doppler data streams, six measured with beams between the three vertex spacecraft and two with beams between each of the optical bench pairs on the three spacecraft. We show that generalizations of our previous linear data combinations, now using these twelve one-way Doppler measurements, can cancel the noises of all six lasers and also remove Doppler shifts due to the non-inertial motions of the six optical benches. It is noteworthy that adjacent optical benches need *not* be rigidly connected and that no phase locking of their lasers is required. From the latest LISA estimates for power spectra of remaining Doppler noises (very-low-level proof-mass ''acceleration'' noise, photodetector shot noise, and beam pointing noise) we compute the sensitivities of the generalized data combinations X and P. In the Appendix we give defining equations and sensitivity results for two additional data combinations, denoted E and U. Like X and P, these combinations only require data from four one-way laser links between the LISA spacecraft. LISA can achieve the desired gravitational wave strain performance of $\sim 10^{-23}$ with any of these combinations.

PACS number(s): 04.80.Nn, 07.60.Ly, 95.55.Ym

I. INTRODUCTION

Very high-sensitivity ground-based Michelson interferometers for the detection and study of high-frequency ($\sim$10–1000 Hz) astrophysical gravitational waves will soon become operational. These observatories will have very precisely equal arm lengths, allowing the direct cancellation of the leading noise source, laser frequency instability. Longer arm-length interferometric detectors in space, e.g. the Laser Interferometer Space Antenna (LISA; [1]), could be operational within the decade and will be sensitive to much lower frequency ($\sim$millihertz) gravitational radiation. Unlike the ground detectors, LISA cannot maintain precise arm-length equality and, because of its size ($\approx 5\times 10^6$ km arms), time-of-flight of laser signals and gravitational waves throughout the apparatus are important. The spacecraft cannot be inertially isolated, but incorporate drag-free proof masses.

We previously treated time-delay gravitational wave interferometry (references [2]; [3], hereafter papers I and II, respectively) with three spacecraft, each idealized as moving almost inertially and each *rigidly* carrying a laser, beam splitters and analyzer photodetectors. Each spacecraft transmits laser signals to the other two and, using its laser as a local oscillator, measures the frequencies of the laser beams received from the other two. In papers I and II we presented and analyzed time-delayed combinations of these data streams which eliminated the dominant noise source, viz. frequency fluctuations of the lasers, while retaining the gravitational wave signal.

In this paper we extend those results by presenting delay equations for data from the actual drag-free configuration envisaged for the LISA project (see Fig. 2, adapted from [1] and [4]). At each vertex spacecraft there are *two* rigid optical benches shielding two (almost) inertial proof masses. Each optical bench has its own laser which is used both to exchange signals with one of the distant spacecraft and also to exchange signals with the adjacent optical bench. Thus there are six optical benches, six lasers, and a total of twelve Doppler time series observed. The six beams exchanged between distant spacecraft contain the gravitational wave signal (plus noises); the other six beams are for comparison of the lasers and relative optical bench motions within each spacecraft. All beams are inertially referenced by reflection off a proof mass. We show here how suitable time-delayed combinations of these twelve data series can recover all the results of paper II, removing now not only the phase noises of the six lasers but also eliminating the Doppler shifts due to non-inertial motions of the spacecraft (i.e., the optical benches).

It is noteworthy that adjacent optical benches need not be rigidly connected and that, although it has been discussed

*Electronic address: Frank.B.Estabrook@jpl.nasa.gov
†Electronic address: Massimo.Tinto@jpl.nasa.gov
‡Electronic address: John.W.Armstrong@jpl.nasa.gov

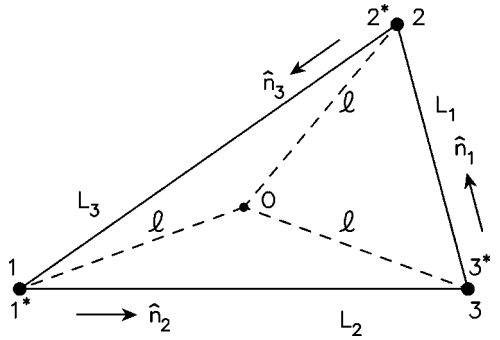

FIG. 1. Schematic LISA configuration. Each spacecraft is equidistant from the point O, in the plane of the spacecraft. Unit vectors $\hat{n}_i$ point between spacecraft pairs with the indicated orientation. At each vertex spacecraft there are two optical benches (denoted 1, 1*, etc.), as indicated.

(e.g., [4]), no phase locking of their lasers, or further direct displacement monitoring of the proof masses, is required. The twelve one-way data streams alone carry all the needed information.

We calculate the gravitational wave sensitivities of the new data combinations. As in papers I and II, gravitational wave sensitivity is limited by shot-noise in the readouts and by acceleration noise in the drag-free system. Despite the apparent complexity, the sensitivities we calculate for the drag-free spacecraft model shown in Fig. 2 are nearly identical to those of the idealized case analyzed in papers I and II.

Time-delay equations for the drag-free data are given in Sec. II. In Sec. III we give the new laser-and-spacecraft-motion-free data combinations. In Sec. IV we briefly discuss the responses of the combinations to incident gravitational waves, and present the gravitational wave sensitivities of the various data combinations. In Sec. V we discuss the required accuracy for knowledge of spacecraft separations and timing of the recorded data streams. In the Appendix we give defining equations and results for two additional data combinations which also require only four laser links between the spacecraft.

II. ANALYSIS

Figure 1 shows the overall geometry of the LISA detector. The spacecraft are labeled 1, 2, 3 and distances between pairs of spacecraft are L_1, L_2, L_3, with L_i being opposite spacecraft *i*. Unit vectors between spacecraft are $\hat{n}_i$, oriented as indicated in Fig. 1. We similarly index the Doppler data to be analyzed: y_{31} is the (fractional or normalized by center frequency—we omit this qualifier in the rest of this paper) Doppler series derived from reception at spacecraft 1 with transmission from spacecraft 2. Similarly, y_{21} is the Doppler time series derived from reception at spacecraft 1 with transmission at spacecraft 3. The other four Doppler time series from signals exchanged between the spacecraft are obtained by cyclic permutation of the indices: $1\rightarrow 2\rightarrow 3\rightarrow 1$. We also use a useful notation for delayed data streams: $y_{31,2}=y_{31}(t-L_2)$, $y_{31,23}=y_{31}(t-L_2-L_3)=y_{31,32}$, etc. (We take c = 1 for the analysis; we use physical units in the calculation of gravitational wave sensitivities). Six more Doppler series result from laser beams exchanged between adjacent optical benches; these are similarly indexed as z_{ij} (i,j = 1, 2, 3.)

The proof-mass-plus-optical-bench assemblies for LISA spacecraft number 1 are shown schematically in Fig. 2. We take the left-hand optical bench to be bench number 1, while the right-hand bench is 1*. The photodetectors that generate the data y_{21}, y_{31}, z_{21}, and z_{31} at spacecraft 1 are shown. The fractional frequency fluctuations of the laser on optical bench 1 is $C_1(t)$; on optical bench 1* it is $C_1^*(t)$ and these are independent (the lasers are not ''locked''). We extend the cyclic terminology of paper II in that at vertex i (i = 1, 2, 3) the random velocities of the two proof masses are respectively denoted $\vec{v}_i(t)$ and $\vec{v}_i^*(t)$, and the random velocities (perhaps several orders of magnitude greater) of their optical benches are correspondingly denoted $\vec{V}_i(t)$ and $\vec{V}_i^*(t)$. (Thus paper II considered the case $\vec{V}_i=\vec{v}_i=\vec{V}_i^*=\vec{v}_i^*$.) Note that

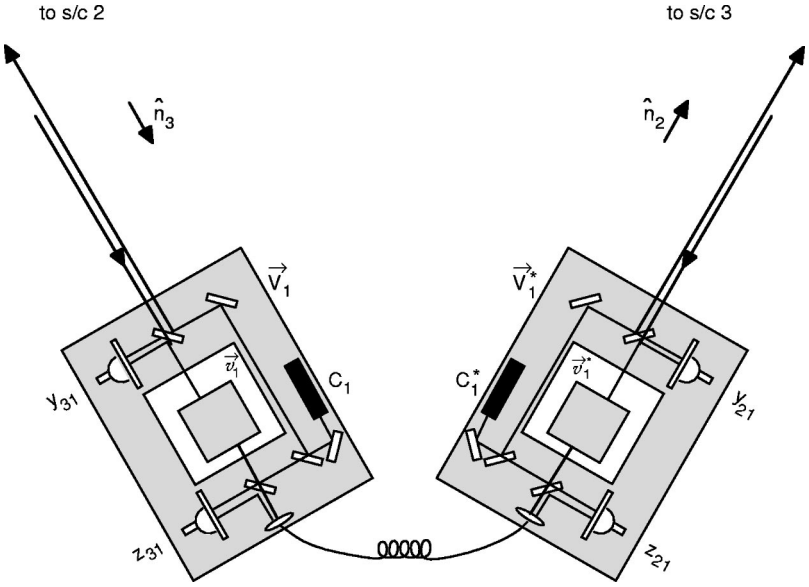

FIG. 2. Schematic diagram, adapted from Refs. [1] and [4], of proof-masses-plus-optical-benches for a LISA spacecraft. The left-hand bench reads out the Doppler signals y_{31} (from spacecraft 2, bounced off the left proof mass, read out using laser and photodetector on the left optical bench) and z_{31} (from the right optical bench, bounced off the right-hand proof mass, redirected to the left-hand bench, and read out with the laser-photodetector on the left bench). The right hand bench analogously reads out y_{21} and z_{21}. The random velocities of the two proof masses and two optical benches are indicated (lower case $\vec{v}_i$ for the proof masses, upper case $\vec{V}_i$ for the optical benches.)

our analysis in this paper does *not* assume that pairs of optical benches are rigidly connected, i.e. $\vec{V}_i \neq \vec{V}_i^*$, in general. The present LISA design shows optical fibers transmitting signals between adjacent benches. We ignore time-delay effects for these signals and will simply denote by $\eta_i(t)$ the frequency shifts upon transmission through the fibers (ultimately due to a component of the relative bench motions, $\vec{V}_i - \vec{V}_i^*$). The $\eta(t)$ frequency shift within a given spacecraft is the same for both local beams, positive if the benches are approaching and negative if separating.

Figure 2 endeavors to make the detailed light paths for these observations clear. An outgoing light beam transmitted to a distant spacecraft is routed from the laser on the local optical bench using mirrors and beam splitters; this beam does not interact with the local proof mass. Conversely, an *incoming* light beam from a distant spacecraft is bounced off the local proof mass before being reflected onto the photodetector where it is mixed with light from the laser on that same optical bench. These data are denoted y_{31} and y_{21} in Fig. 2. Beams between adjacent optical benches however do precisely the opposite. Light to be *transmitted* from the laser on an optical bench is *first* bounced off the proof mass it encloses and then directed to the other optical bench. Upon reception it does *not* interact with the proof mass there, but is directly mixed with local laser light. These data are denoted z_{31} and z_{21} in Fig. 2. This very clever configuration is due to the insight of the original designers [1,5] and, as will appear, allows the twelve Doppler data streams to be combined so as to eliminate all laser phase noises (C_i and C_i^*) and optical bench buffeting ($\vec{V}_i$ and $\vec{V}_i^*$) noises from generalizations of all the data combinations given in paper II.

The terms in the following equations for the y_{ij} and z_{ij} Doppler measurements can now be developed from Figs. 1 and 2. Consider equation (2.3). The y_{31} photodetector on the left bench of spacecraft 1, moving with velocity $\vec{V}_1$, reads the Doppler signal y_{31} by mixing the beam originating from the distant optical bench 2^* in direction $\hat{n}_3$ (laser noise C_2^* and optical bench motion $\vec{V}_2^*$, delayed by propagation along L_3), after one bounce off the proof mass ($\vec{v}_1$), with the local laser light (C_1). In Eq. (2.4) the z_{31} measurement results from light originating at the right-bench laser (C_1^*, $\vec{V}_1^*$), bounced once off the right proof mass ($\vec{v}_1^*$), and directed through the fiber [incurring Doppler shift $\eta_1(t)$], to the left bench, where it is mixed with laser light (C_1). Similarly the right bench records Doppler observations y_{21} and z_{21}. The four photodetector readouts at vertex 1, including gravitational wave signals and shot noises as in paper II, are thus

$$y_{21} = C_{3,2} - \hat{n}_2 \cdot \vec{V}_{3,2} + 2\hat{n}_2 \cdot \vec{v}_1^* - \hat{n}_2 \cdot \vec{V}_1^* - C_1^* + y_{21}^{gw} + y_{21}^{shot} \tag{2.1}$$

$$z_{21} = C_1 + 2\hat{n}_3 \cdot (\vec{v}_1 - \vec{V}_1) + \eta_1 - C_1^* \tag{2.2}$$

$$y_{31} = C_{2,3}^* + \hat{n}_3 \cdot \vec{V}_{2,3}^* - 2\hat{n}_3 \cdot \vec{v}_1 + \hat{n}_3 \cdot \vec{V}_1 - C_1 + y_{31}^{gw} + y_{31}^{shot} \tag{2.3}$$

$$z_{31} = C_1^* - 2\hat{n}_2 \cdot (\vec{v}_1^* - \vec{V}_1^*) + \eta_1 - C_1 . \tag{2.4}$$

Eight other relations, for the readouts at vertices 2 and 3, are given by cyclic permutation of the indices in Eqs. (2.1)–(2.4). The gravitational wave signal components in Eqs. (2.1) and (2.3) are given by Eqs. (1)–(3) of paper II. The shot noise contributions, y_{ij}^{shot}, due to the low signal-to-noise ratio (SNR) in the links connecting the distant spacecraft, are also given in paper II. The z_{ij} measurements will be made with high SNR so that shot noise is negligible.

III. DATA COMBINATIONS WHICH ELIMINATE LASER NOISES AND OPTICAL BENCH MOTIONS

The data combinations appropriate for LISA can now readily be obtained from those given in paper II. Inserting Eqs. (2.1) and (2.3) in the expressions given in paper II it is almost immediate to see the additional terms in Eqs. (2.2) and (2.4) required to eliminate both C_i and C_i^*. If the z_{ij} are taken only in the combinations $z_{21} - z_{31}$, $z_{32} - z_{12}$, $z_{13} - z_{23}$ the η_i also drop out. The modified combinations are given next; they retain only proof mass motions $\vec{v}_i^*$ and $\vec{v}_i$ (acceleration noise) and readout errors (shot noise). The combinations are not independent, but span a three-dimensional function space. The various time-delay relations between the combinations given in paper II are still exactly true for the final combinations appropriate for LISA (involving the z_{ij}).

A. Unequal-arm-length interferometric combinations

We showed in paper I how to appropriately combine time-domain data from the two arms of each of the three possible interferometers in the array so as to cancel exactly laser noise. This method was also discussed as the laser-noise-free data combinations X, Y, and Z in paper II. When modified for the drag-free LISA configuration the unequal-arm-length interferometric combination X is now

$$\begin{aligned} X = {} & y_{32,322} - y_{23,233} + y_{31,22} - y_{21,33} + y_{23,2} - y_{32,3} + y_{21} - y_{31} \\ & + \frac{1}{2}(-z_{21,2233} + z_{21,33} + z_{21,22} - z_{21}) \\ & + \frac{1}{2}(+z_{31,2233} - z_{31,33} - z_{31,22} + z_{31}). \end{aligned} \tag{3.1}$$

Combinations Y and Z follow from cyclic permutation of the indices. Explicit substitution of Eqs. (2.1)–(2.4) in the above, verifies that all six laser phase noises (the C_i and C_i^*) and all six optical bench motions (the V_i and V_i^*) cancel exactly. The gravitational wave signal is preserved as a superposition of eight realizations and is given by Eq. (24) of paper II. The remaining noise terms due to proof-mass motions, $\vec{v}_i$ and $\vec{v}_i^*$, are

$$\begin{aligned} X^{proof\ mass} = {} & \hat{n}_2 \cdot (-\vec{v}_{1,2233}^* + \vec{v}_{1,22}^* - \vec{v}_{1,33}^* + \vec{v}_1^* \\ & + 2\vec{v}_{3,233} - 2\vec{v}_{3,2}) + \hat{n}_3 \cdot (-\vec{v}_{1,2233} + \vec{v}_{1,33} \\ & - \vec{v}_{1,22} + \vec{v}_1 + 2\vec{v}_{2,223}^* - 2\vec{v}_{2,3}^*). \end{aligned} \tag{3.2}$$

B. The α, β, γ combinations

Another three independent linear combinations of the Doppler data which do not contain laser or optical bench noises are

$$\alpha = y_{21} - y_{31} + y_{13,2} - y_{12,3} + y_{32,12} - y_{23,13} - \frac{1}{2}(z_{13,2} + z_{13,13} + z_{21} + z_{21,123} + z_{32,3} + z_{32,12}) + \frac{1}{2}(z_{23,2} + z_{23,13} + z_{31} + z_{31,123} + z_{12,3} + z_{12,12}) \quad (3.3)$$

with β, and γ given, as usual, by cyclical permutation of the indices. A δ-function gravitational wave excitation produces six pulses in α, with relative times depending on the arrival direction of the wave and the detector geometrical configuration [3]. Noninertial motions of the proof-masses do not cancel; this contribution to α is

$$\alpha^{proof\ mass} = \hat{n}_1 \cdot (\vec{v}_{2,3} - \vec{v}_{2,12} + \vec{v}^*_{3,2} - \vec{v}^*_{3,13}) + \hat{n}_2 \cdot (\vec{v}_{3,13} - \vec{v}_{3,2} + \vec{v}^*_1 - \vec{v}^*_{1,123}) + \hat{n}_3 \cdot (\vec{v}_1 - \vec{v}_{1,123} + \vec{v}^*_{2,12} - \vec{v}^*_{2,3}). \quad (3.4)$$

C. Fully symmetric (Sagnac) combination

A symmetric data combination which exactly cancels all laser and optical bench motion noises and has the property that each of the y_{ij} enters exactly once and is lagged by exactly one of the one-way light times is ζ:

$$\zeta = y_{32,2} - y_{23,3} + y_{13,3} - y_{31,1} + y_{21,1} - y_{12,2} + \frac{1}{2}(-z_{13,21} + z_{23,12} - z_{21,23} + z_{31,23} - z_{32,13} + z_{12,13}) + \frac{1}{2}(-z_{32,2} + z_{12,2} - z_{13,3} + z_{23,3} - z_{21,1} + z_{31,1}). \quad (3.5)$$

Like α, β, γ, this combination also has a six-pulse response to gravitational radiation [3].

The proof-mass noise for ζ is

$$\zeta^{proof\ mass} = \hat{n}_1 \cdot (\vec{v}_{2,2} - \vec{v}_{2,13} + \vec{v}^*_{3,3} - \vec{v}^*_{3,21}) + \hat{n}_2 \cdot (\vec{v}_{3,3} - \vec{v}_{3,21} + \vec{v}^*_{1,1} - \vec{v}^*_{1,23}) + \hat{n}_3 \cdot (\vec{v}_{1,1} - \vec{v}_{1,23} + \vec{v}^*_{2,2} - \vec{v}^*_{2,13}). \quad (3.6)$$

D. Combinations with data taken at two spacecraft

An interesting set of laser-and-optical-bench-noise-free data combinations involve data taken at only two spacecraft [3]. These combinations have obvious utility in the event of receiver failure at one spacecraft and also have gravitational wave sensitivities very similar to those of the unequal arm interferometer (X, Y, Z) combinations of the baseline LISA design (see [3] and below). The P, Q, R combinations which cancel laser and bench motion noises are

$$P = y_{32,2} - y_{23,3} - y_{12,2} + y_{13,3} + y_{12,13} - y_{13,12} + y_{23,311} - y_{32,211} + \frac{1}{2}(-z_{21,23} + z_{21,1123} + z_{31,23} - z_{31,1123}) + \frac{1}{2}(-z_{32,2} + z_{32,112} + z_{12,2} - z_{12,112}) + \frac{1}{2}(-z_{13,3} + z_{13,113} + z_{23,3} - z_{23,113}) \quad (3.7)$$

with Q and R given by index permutation. The proof mass noise contribution is

$$P^{proof\ mass} = \hat{n}_1 \cdot (\vec{v}_{2,2} - 2\vec{v}_{2,13} + \vec{v}_{2,112} + \vec{v}^*_{3,3} - 2\vec{v}^*_{3,12} + \vec{v}^*_{3,113}) + \hat{n}_2 \cdot (-\vec{v}^*_{1,23} + \vec{v}^*_{1,1123} + \vec{v}_{3,3} - \vec{v}_{3,311}) + \hat{n}_3 \cdot (-\vec{v}_{1,23} + \vec{v}_{1,1123} + \vec{v}^*_{2,2} - \vec{v}^*_{2,112}). \quad (3.8)$$

IV. SENSITIVITY TO GRAVITATIONAL WAVES

Since the LISA arm lengths will differ by at most a few percent, we specialize now to the equilateral-triangle case $L_1 = L_2 = L_3 = L$, with $L = 10\sqrt{3}$ light seconds. To compute sensitivity we need the power spectra of the principal noise sources and their transfer functions to the data combinations (X, α, etc.) being considered. We take the shot noise spectrum for an individual y_{ij} laser link to be $S_y^{shot} = 5.3 \times 10^{-38}\ (f/1\ \mathrm{Hz})^2\ \mathrm{Hz}^{-1}$ (Ref. [1]). Acceleration noise for an individual proof mass is currently expected (Ref. [1], Table 4.2) to have a spectrum $S_y^{proof\ mass} = 2.5 \times 10^{-48}[f/1\ \mathrm{Hz}]^2\ \mathrm{Hz}^{-1}$. The transfer functions of the proof mass noise are given in Eqs. (3.2), (3.4), (3.6), and (3.8). Shot noises enter only in the y_{ij}, so their contributions to the generalized linear combinations given here are the same as for the corresponding linear combinations in paper II. In the sensitivity plots presented in this paper, we approximately account for all optical-path noise, including beam pointing noise, through a spectrum $S_y^{optical\ path} = 1.8 \times 10^{-37}\ (f/1\ \mathrm{Hz})^2$ (Ref. [1], Table 4.1), and take this aggregate to have the same transfer function as shot noise alone. Thus the noise spectra used here are slightly different than those used for sensitivity calculations in paper II. The resulting power spectra of the acceleration and shot noise components of X, α, ζ, and P, assuming independent individual proof mass acceleration noises and independent shot noises, are

$$S_X = [8\sin^2(4\pi fL) + 32\sin^2(2\pi fL)]S_y^{proof\ mass} + 16\sin^2(2\pi fL)S_y^{optical\ path} \quad (4.1)$$

$$S_\alpha = [8\sin^2(3\pi fL) + 16\sin^2(\pi fL)]S_y^{proof\ mass} + 6S_y^{optical\ path} \quad (4.2)$$

$$S_\zeta = 24\sin^2(\pi fL)S_y^{proof\ mass} + 6S_y^{optical\ path} \quad (4.3)$$

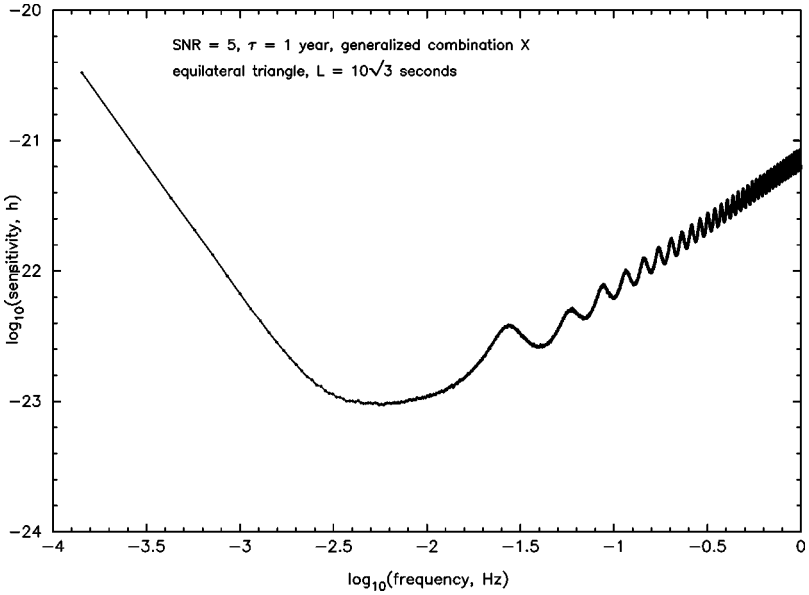

FIG. 3. Sensitivity calculation for the laser-and-optical-bench-noise-free combination, X [Eq. (3.1)], as a function of Fourier frequency, for the equilateral triangle LISA case (L = 17.32 light seconds). Sensitivity is for SNR = 5 in a one year integration time, averaging over the celestial sphere and over general elliptical polarization state. [Noise spectra used for proof-mass accelerations (3×10^{-15} (m/sec^2) Hz$^{-1/2}$) and aggregate optical path noise (20×10^{-12} m Hz$^{-1/2}$) are from Ref. [1], appropriately converted to power spectra for single-link Doppler observations; see text.]

$$S_P=[8\sin^2(2\pi fL)+32\sin^2(\pi fL)]S_y^{proof\ mass}+[8\sin^2(2\pi fL)+8\sin^2(\pi fL)]S_y^{optical\ path}. \tag{4.4}$$

These can be compared with similar noise transfer function expressions derived for the idealized case in paper II.

Gravitational wave sensitivity is the wave amplitude required to achieve a given signal-to-noise ratio. We calculate it in the conventional way [1], requiring a signal-to-noise ratio of 5 in a one year integration time: $5\sqrt{S_k(f)B}$/(rms gravitational wave response for data combination k), where k is α, ζ, X, P, etc. and S_k is the total noise power spectrum. The bandwidth, B, was taken to be 3.17×10^{-8} Hz (i.e., one cycle/year). We averaged over source direction (assumed uniformly distributed on the celestial sphere) and elliptical polarization state (assumed uniformly distributed on the Poincaré sphere for each source direction). The averaging was done by a Monte Carlo simulation with 2500 source position/polarization state pairs per Fourier frequency bin and 7000 Fourier bins across the LISA band ($\sim10^{-4}$ Hz to $\sim10^{-1}$ Hz); see paper II. Figures 3 and 4 show the sensitivities for linear combinations X and P. [Schilling (1997) [6] modeled LISA as a rigid, equal-arm one-bounce conventional interferometer. His independent sensitivity calculation, which used slightly different noise spectra, should be compared with ours for X.]

V. ARM LENGTH KNOWLEDGE AND TIMING ACCURACY

A limitation on the procedure described above, however, may come from non-cancelled laser noise affecting the Doppler data due to inaccuracies in the determination of the distances between the three pairs of spacecraft, and the synchro-

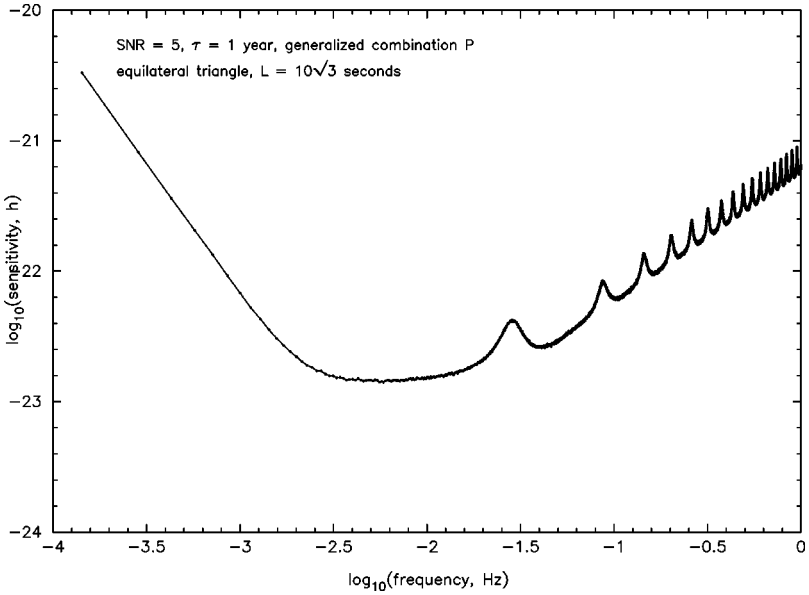

FIG. 4. As in Fig. 3, but for the laser-and-optical-bench-noise-free combination, P [Eq. (3.7)].

nization of the three clocks that time-tag the Doppler data on board each spacecraft.

Since the frequency drifts of these three clocks can be neglected over time scales equal to a few round-trip-light-times, it follows that pairs of clocks can be synchronized to a level identified by the accuracy of the arm length measurement (e.g., [7]). If we define $\Delta\tau_i$ $i=1,2,3$ to be the accuracies of the local clocks, it is easy to derive the spectral density of the non-cancelled noise due to the frequency fluctuations of the lasers in any of the data combinations analyzed in the previous sections. If we take the spectral densities of the frequency fluctuations of the six lasers to be $S_c(f)$, the spectral density of the remaining laser noise in the X combination is

$$32\pi^2 f^2 S_c(f)[\sin^2(2\pi f L_2)(\Delta L_3^2+(\Delta\tau_2-\Delta\tau_1)^2) + \sin^2(2\pi f L_3)(\Delta L_2^2+(\Delta\tau_3-\Delta\tau_1)^2)]. \quad (5.1)$$

Assuming $\Delta L_1 \approx \Delta\tau_2-\Delta\tau_3$, etc., and $L_1=L_2=L$, this reduces to

$$\approx 64\pi^2 f^2 S_c(f)\sin^2(2\pi f L)(\Delta L_2^2+\Delta L_3^2). \quad (5.2)$$

Requiring this spectral density to be smaller than the spectra of the proof-mass and shot noise puts upper limits on arm length and clock synchronization errors.

The issue of arm length accuracy has previously been discussed in paper I for unequal arm-length *transponding* interferometers; timing accuracy did not enter since data were taken at a single spacecraft. We can recover that result by imposing the conditions for transponding at spacecraft 2 and 3, and for laser phase-locking at spacecraft 1: $y_{32}=y_{23}=0$ and $z_{21}-z_{31}=0$. Whether these can in fact be achieved by onboard electronics, to the required precision ($\sim 10^{-23}$) may need to be demonstrated. Using these conditions in Eqs. (3.1) eliminates the fluctuation noises of all but one laser, which however then appears four times in X, correlated. The resulting noise power, in the nominally equal arm case, now depends on $(\Delta L_2-\Delta L_3)^2$:

$$64\pi^2 f^2 S_c(f)\sin^2(2\pi f L)(\Delta L_2-\Delta L_3)^2. \quad (5.3)$$

The numerical arm-length tolerance for linear combination X is thus comparable to that for a transponding interferometer, ≈ 30 meters for the nominal LISA configuration and nominal noise power spectra (paper I).

VI. SUMMARY AND CONCLUSIONS

We have given a general treatment of the principal noise sources for an unequal arm space-borne gravitational wave detector such as LISA. Our analysis included acceleration noises of the six proof masses in the realistic LISA configuration, the laser signals exchanged between the vertex spacecraft, and the signals exchanged between optical benches–proof masses within each spacecraft.

The instrument was analyzed in terms of twelve observable one-way Doppler time series (six between pairs of spacecraft; six between optical benches within spacecraft). We showed here that generalizations of the data combinations given in paper II cancel all six laser noises and the motions of all six optical benches while preserving gravitational wave signals. Our analysis was general: we did *not* assume that the two optical benches within a spacecraft were rigidly connected and we did *not* require that the various lasers be phase-locked. These generalizations of the laser-and-optical-bench-motion noise-free linear combinations X, α, ζ, P, etc. thus offer the same flexibility and potential advantages (e.g. in hardware design, in robustness to failures of single links, and in redundancy in data analysis) as the analogous combinations given earlier. We derived transfer functions of the noise to these generalized data combinations and used them to compute aggregate noise spectra and gravitational wave sensitivity. The requirements on arm length accuracy (and corresponding clock synchronization) were found to be closely comparable to those for a transponding interferometer.

ACKNOWLEDGMENTS

We thank William Folkner and Peter Bender for valuable discussions regarding the LISA detector. This research was performed at the Jet Propulsion Laboratory, California Institute of Technology, under contract with the National Aeronautics and Space Administration.

APPENDIX: EIGHT PULSE DATA COMBINATIONS

We have seen that the interferometric combinations X, Y, Z are not the only reduced data involving a subset (four) of the six y_{ij} that eliminate all laser and optical bench phase noise. The combinations P, Q, R also involve four streams of data, taken at two spacecraft with the third only transmitting, providing an independent frequency ''beacon.'' There are two additional combinations of only four y_{ij} that are free of laser and optical bench phase noises that should also be noted for completeness.

Otherwise said, there are four different combinations of

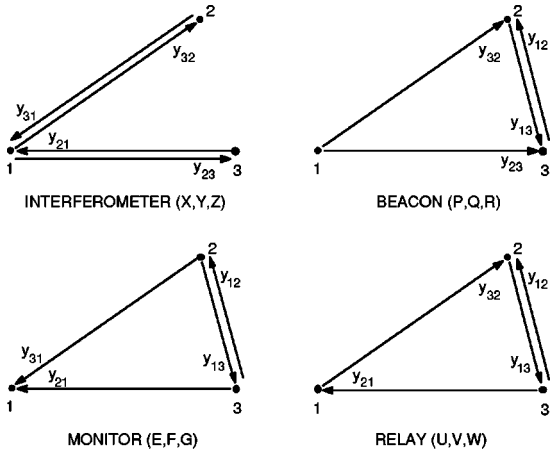

FIG. 5. Schematic diagram of LISA configurations (interferometric, beacon, monitor, and relay) involving only four links. The diagram shows X, P, E, and U with the others in each class determined from cyclic permutation of indices as discussed in the text. All yield eight-pulse responses to gravitational waves.

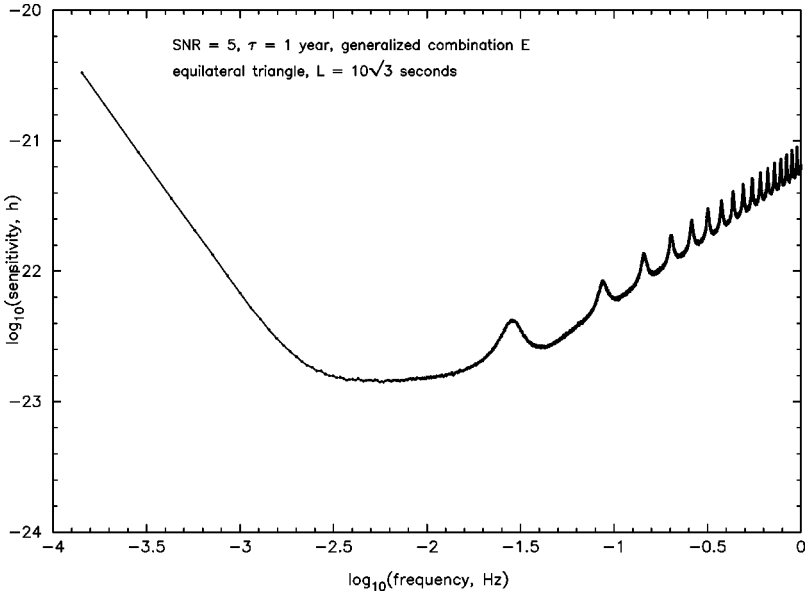

FIG. 6. As in Fig. 3, but for the ''monitor'' laser-and-optical-bench-noise-free combination, E [Eq. (A1)].

one-way data streams to use in the event that one or two laser links are not available The alternatives are illustrated in Fig. 5; the combinations are denoted respectively ''interferometer,'' ''beacon,'' ''monitor'' and ''relay.'' The last three of these names reflect the remaining function of the third spacecraft. In all cases in the resulting reduced data stream there is an 8-pulse response to an incident gravitational wave pulse.

The X, Y, Z and P, Q, R cases have been discussed above. Expressions for the monitor (E, F, G, say) and relay (U, V, W) combinations, their responses to gravitational waves and proof mass motions, and the resulting LISA proof-mass and shot noise spectra are next given, with our usual cyclic notation convention.

1. Monitor combinations (E, F, G)

The monitor combination E is illustrated in Fig. 5. E is $\alpha-\zeta_{,1}$ and is explicitly constructed as

$$E = y_{12,21} - y_{13,31} - y_{12,3} + y_{13,2} + y_{31,11} - y_{21,11} - y_{31} + y_{21} - \frac{1}{2}(z_{13,2} + z_{21} + z_{32,3} - z_{13,112} + z_{23,112} - z_{32,113}) + \frac{1}{2}(z_{23,2} + z_{31} + z_{12,3} - z_{12,113} + z_{21,11} - z_{31,11}). \quad \text{(A1)}$$

The gravitational wave response is implicit from $E=\alpha-\zeta_{,1}$, using the gravitational wave contributions to α and ζ given in Eqs. (15) and (18) of paper II. The transfer function of proof-mass noise to E is

$$E^{proof\ mass} = \hat{n}_1\cdot(\vec{v}_{2,3} - 2\vec{v}_{2,12} + \vec{v}_{2,113} + \vec{v}^{\,*}_{3,2} - 2\vec{v}^{\,*}_{3,13} + \vec{v}^{\,*}_{3,112}) + \hat{n}_2\cdot(-\vec{v}_{3,2} + \vec{v}_{3,112} + \vec{v}^{\,*}_{1} - \vec{v}^{\,*}_{1,11}) + \hat{n}_3\cdot(\vec{v}_{1} - \vec{v}_{1,11} - \vec{v}^{\,*}_{2,3} + \vec{v}^{\,*}_{2,113}). \quad \text{(A2)}$$

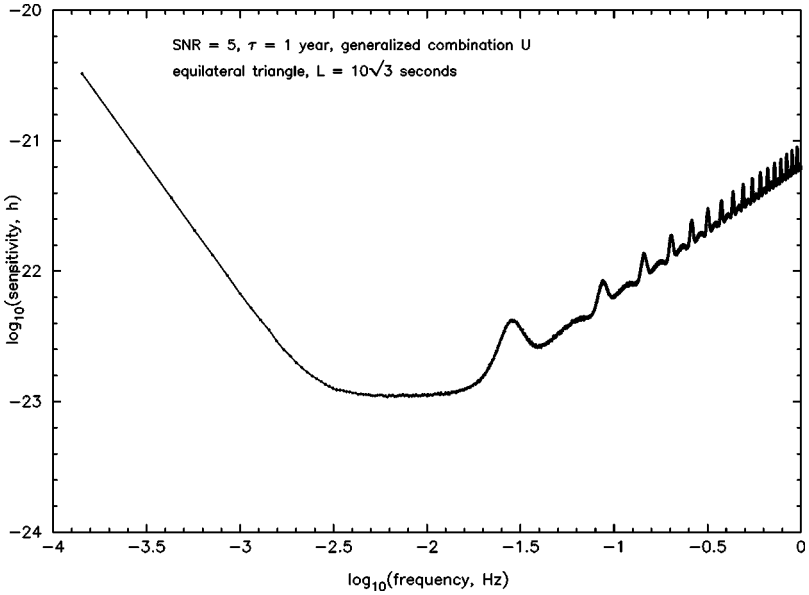

FIG. 7. As in Fig. 3, but for the ''relay'' laser-and-optical-bench-noise-free combination, U [Eq. (A4)].

As before, the shot noise enters only in the y_{ij}. The power spectra of the acceleration and shot noise components of E, assuming independent individual proof mass acceleration noises and independent shot noises, is

$$S_E = [32\sin^2(\pi fL) + 8\sin^2(2\pi fL)]S_y^{proof\ mass} + [8\sin^2(\pi fL) + 8\sin^2(2\pi fL)]S_y^{optical\ path}. \tag{A3}$$

2. Relay combinations (U, V, W)

The relay combination U is illustrated in Fig. 5. U is $\gamma_{,1} - \beta$:

$$U = y_{21,113} - y_{21,3} - y_{12,123} + y_{13,1} - y_{13,23} + y_{32,11} - y_{32} + y_{12} - \frac{1}{2}(z_{31,3} + z_{12} + z_{23,23} + z_{32,11} + z_{13,1123} + z_{21,113}) + \frac{1}{2}(z_{21,3} + z_{32} + z_{13,23} + z_{12,11} + z_{23,1123} + z_{31,113}). \tag{A4}$$

The gravitational wave response is implicit from $U = \gamma_{,1} - \beta$, using the gravitational wave contributions to γ and β given in Eq. (15) of paper II, with appropriately cyclical permutation of indices. The transfer function of proof-mass noise to U is

$$U^{proofmass} = \hat{n}_1 \cdot (2\vec{v}_{2,123} - \vec{v}_{2,11} - \vec{v}_2 - \vec{v}^*_{3,1123} - \vec{v}^*_{3,23} + 2\vec{v}^*_{3,1}) + \hat{n}_2 \cdot (\vec{v}_{3,23} - \vec{v}_{3,1123} - \vec{v}^*_{1,3} + \vec{v}^*_{1,113}) + \hat{n}_3 \cdot (\vec{v}_{1,3} - \vec{v}_{1,113} - \vec{v}^*_2 + \vec{v}^*_{2,11}). \tag{A5}$$

The power spectra of acceleration and shot noise components of U (with independent individual proof mass and shot noises) is

$$S_U = [16\sin^2(\pi fL) + 8\sin^2(2\pi fL) + 16\sin^2(3\pi fL)]S_y^{proof\ mass} + [4\sin^2(\pi fL) + 8\sin^2(2\pi fL) + 4\sin^2(3\pi fL)]S_y^{optical\ path}. \tag{A6}$$

The LISA sensitivity curves are given in Figs. 3 and 4 (for X and P, respectively) and Figs. 6 and 7 (for E and U, respectively). They are all very similar.

[1] P. Bender *et al.*, ''Laser Interferometer Space Antenna for the Detection of Gravitational Waves,'' Pre-Phase A Report, MPQ 233, Max-Planck-Institüt für Quantenoptik, Garching, 1998.

[2] M. Tinto and J. W. Armstrong, Phys. Rev. D **59**, 102003 (1999), paper I.

[3] J. W. Armstrong, F. B. Estabrook, and M. Tinto, Astrophys. J. **527**, 814 (1999), paper II.

[4] M. Peterseim, D. I. Robertson, K. Danzmann, H. Welling, and P. Bender, Adv. Space Res. **25**, 1143 (2000).

[5] R. W. Hellings *et al.*, ''Mission Concept Study for SAGITTARIUS,'' JPL Engineering Memorandum 314-569 (1993).

[6] R. Schilling, Class. Quantum Grav. **14**, 1513 (1997).

[7] J. C. Camparo, R. P. Frueholz, and A. P. Dubin, in *Demonstration of Synchronization Between Two Geosynchronous Satellites Without Ground Intervention*, Proceedings of the 28th Annual Precise Time and Time Interval (PTTI) Applications and Planning Meeting, edited by L. A. Breakiron (The US Naval Observatory, Washington, DC, 1996).